Revisiting the Empirical Fundamental Relationship

Benjamin Coifman, PhD

Associate Professor
The Ohio State University
Joint appointment with the Department of Civil, Environmental, and Geodetic Engineering, and the Department of Electrical and Computer Engineering

Hitchcock Hall 470
2070 Neil Ave, Columbus, OH 43210
Phone: (614) 292-4282
E-mail: Coifman.1@OSU.edu

Abstract

This paper develops a new methodology for deriving an empirical fundamental relationship from vehicle detector data. The new methodology seeks to address several sources of noise present in conventional measures of the traffic state that arise from the data aggregation process, e.g., averaging across all vehicles over a fixed time period. In the new methodology vehicles are no longer taken successively in the order in which they arrived and there is no requirement to seek out stationary traffic conditions; rather, the traffic state is measured over the headway for each individual vehicle passage and the vehicles are grouped by similar lengths and speeds before aggregation. Care is also taken to exclude measurements that might be corrupted by detector errors. The result is a homogeneous set of vehicles and speeds in each bin. While conventional fixed time averages may have fewer than 10 vehicles in a sample, the new binning process ensures a large number of vehicles in each bin before aggregation. We calculate the median flow and median occupancy for each combined length and speed bin. Then we connect these median points across all of the speed bins for a given vehicle length to derive the empirical fundamental relationship for that length. This use of the median is also important; unlike conventional aggregation techniques that find the average, the median is far less sensitive to outliers arising from uncommon driver behavior or occasional detector errors.

The work is applied to real data from a dual loop detector station and it yields consistent results across 18 independent days, 4 independent lanes, and 7 independent length bins. These empirical results from non-stationary traffic are also shown to be consistent with hypothetical results generated with homogeneous vehicles under stationary traffic conditions.

Keywords

Fundamental relationship, loop detectors, highway traffic

1. Introduction

This paper develops a new methodology for deriving an empirical fundamental relationship (FR) from vehicle detector data. This work is important because much of traffic flow theory depends on the existence of a FR between flow, q, density, k, and space mean speed, v either explicitly, e.g., Lighthill and Whitham (1955), and Richards (1956) (LWR) hydrodynamic model or implicitly, e.g., car following models (Chandler et al., 1958; Gazis et al., 1961). The FR is commonly characterized in terms of a bivariate relationship between two of the three parameters (in each case the third parameter can be calculated from the fundamental equation, repeated in Equation 1). All of the empirically generated FRs use data that average conditions over time and/or space to calculate the traffic state, (q, k, v). It is difficult to measure k directly, so many empirical FR studies use occupancy, occ, as a proxy for k, where: occ is the percentage of the sampling period, T, that vehicles occupy the detector. As shown in Equation 2, in stationary traffic occ is proportional to k by the average effective vehicle length, L_{eff} during T; where a given vehicle's effective length is the sum of its physical length and the size of the detection zone.

$$q = k * v \tag{1}$$
$$occ = k * L_{eff} \tag{2}$$

Most empirical FR studies use traffic state measurements from conventional detectors that average vehicle measurements over fixed time sampling periods. Figure 1A shows the measured q versus occ from one of the dual loop detectors in the Berkeley Highway Laboratory, BHL, (Coifman et al., 2000) on a single lane on a single day[1], using T = 30 sec aggregation periods. The results are typical of 30 sec aggregation periods aside from the fact that this location experienced over 12 hrs of recurring congestion on this day, as per the corresponding time series speed shown in Figure 1D. The q versus occ plot shows considerable scatter and it is hard to imagine any single curve that would be representative of all of the observed data points. The scatter is commonly attributed to combining non-stationary traffic states, e.g., Cassidy (1998), and debate continues as how best to address the scatter.

The choice of T is an effort to balance between maximizing the number of vehicles in the sample and minimizing the averaging across inhomogeneous traffic states. Often setting T = 30 sec is considered to be a good balance between the two competing objectives, though the original use of T = 30 sec appears to have been for the convenience of telecommunications (Gazis and Foote, 1969). Figure 1B repeats the q versus occ for the same vehicles from Figure 1A, only now using T = 5 min. With the longer sample period, each data point in Figure 1B is more likely to combine different non-stationary traffic states, yet the scatter in this plot is diminished compared to T = 30 sec. Thus, the noise in the T = 30 sec plot cannot strictly be due to averaging across non-stationary traffic states. The T = 5 min plot also exhibits plateauing predicted by Hurdle and Datta (1983) and subsequently illustrated in Hsu and Banks (1993): whereby the q versus occ within the queue is truncated at q_P, some maximum q below the bottleneck capacity, due to traffic entering from on-ramps between the detector location and the bottleneck. This downstream demand consumes a portion of the bottleneck capacity and in this case the resulting

[1] These data come from BHL station 6, westbound, lane 4 on December 17, 1997.

plateau in the detector data plot falls around q_P = 1,500 vph, as shown with a dashed line throughout Figure 1.

Conventional fixed time sampling is a crude methodology that was originally designed to smooth out variability across vehicles in an era when computing power was expensive. While it is true that successive vehicles will usually experience similar traffic conditions while traversing the detector, the impacts of differing vehicle properties can far outweigh any benefits that might come from arbitrarily grouping vehicles based on successive passages, e.g., Coifman (2001) and Coifman et al. (2003) showed empirically that the range of feasible vehicle length undermines conventional relationships between q and occ. Coifman (2014) used hypothetical microscopic models to revisit the process of generating empirical FR and uncovered several commonly underappreciated factors that result in surprisingly large, non-linear distortions of the empirical traffic state measurements.

Briefly reviewing Coifman (2014), in general for a fleet of homogeneous vehicles, stationary traffic, in a sample with a large number of vehicles occ is related to k via Equation 2. If one assumes a triangular flow-density FR (denoted qkFR), the curve is uniquely defined by: capacity, q_o, free speed, v_f, and jam density, k_j. Then, extending to the flow-occupancy FR (qoccFR), Equation 3 gives occ_j. The resulting qoccFR is shown on the right-hand side of Figure 2A for a hypothetical example with $v_f = 65\ mph$, $q_o = 2{,}400\ vph$, $k_j = 211\ vpm$ and $L_{eff} = 20\ ft$, while the left-hand side shows the corresponding speed-flow relationship (qvFR), transposed from the commonly used orientation to facilitate direct comparisons between these two forms of the FR.

$$occ_j = k_j * L_{eff} \tag{3}$$

Even under strictly stationary traffic conditions with homogeneous vehicles, Coifman (2014) found that conventional aggregated q, occ and v measurements should exhibit large scatter in the queued regime arising from a combination of:

(a) errors due to a non-integer number of vehicle headways in a given sample,
(b) averaging over a small number of vehicles during low q,
(c) the inclusion of detector errors, and
(d) the mixing of inhomogeneous vehicles within a sample.

Generally the errors grow larger at lower v. Coifman (2014) also found that, unfortunately, the q-occ plane is skewed such that the noisy low-speed samples cover a disproportionately large area. The points in the qvFR on the left-hand side of Figure 2A are plotted at 5 mph intervals and the corresponding states are shown in the qoccFR by projecting horizontally to the curve on the right-hand side of the figure. Proportionately the qoccFR greatly distorts the relationship to v. The dashed lines in Figure 2A show that when speed has dropped from v_f by 38% ($v = 40\ mph$) flow has only dropped from q_o by 10%, and when speed has dropped by 85% ($v = 10\ mph$) flow has only dropped by 49%. In other words, the higher-speed data are compressed into a narrow sliver, e.g., one can see that the highest speeds in the queued regime are compressed to a small range of q (or of occ); while the low-speed data ($v < 10\ mph$) are spread over more than half of the feasible range of q or occ.

There have been numerous past efforts to reduce the scatter in empirical studies and find a representative FR curve. Most of these efforts have focused on identifying homogeneous

periods in conventional aggregated data. Cassidy (1998) is a notable example; it used background subtraction (a form of low pass filtering used to suppress high frequency noise) to identify extended periods with roughly constant q and occ, and for each of these "nearly stationary" periods took a single average q and occ across the underlying sample measurements. Thereby providing a much larger sample size, addressing items (a)-(b). However, any approach that combines aggregate data into even larger samples cannot control for item (d) any better than the original aggregate data. Furthermore, the lowest speed conditions (e.g., occ > 40% in Figure 2A) typically are transient, with stationary conditions lasting less than common sampling periods, and thus, they cannot be resolved by combining multiple sampling periods together.

The findings from Coifman (2014) serve as the starting point for the current paper as we revisit and improve upon the process of generating an empirical FR. Section 2 develops a new sampling methodology designed to address the above shortcomings, (a)-(d), by specifically focusing on the sources of the distortions and minimizing their impacts. Section 3 applies the methodology to real detector data and in the process the section also provides further details of the methodology. Finally, this paper closes in Section 4 with a discussion and conclusions.

2. Methodology

In the this new methodology to derive an empirical FR, vehicles are no longer taken successively in the order in which they arrived and there is no requirement to seek out stationary traffic conditions; rather, each vehicle is measured individually and the vehicles grouped by similar lengths and speeds before aggregation, as discussed this section. First, to eliminate the impacts of non-integer headways in the measured traffic state, individual vehicle headway, h, is measured and then converted to flow during the single vehicle passage (svp) via Equation 4. The associated detector on_time is measured and is used in conjunction with h to calculate occ_{svp} via Equation 5. Obviously the individual q_{svp} and occ_{svp} should be far noisier than conventional fixed time sampled q and occ where vehicles are taken successively. This choice is deliberate; as noted above, rather than attempt to account for the noise at the start, we will address it in a later step. Next, speed and effective vehicle length are measured for each individual vehicle via Equations 6-7.

$$q_{svp} = \frac{1}{h} \tag{4}$$

$$occ_{svp} = \frac{on\_time}{h} * 100\% \tag{5}$$

$$v_{svp} = \frac{detector\_spacing}{traversal\_time} \tag{6}$$

$$L_{svp} = v_{svp} * on\_time \tag{7}$$

To be precise about the details of the calculations, here h is measured rear bumper to rear bumper to ensure that the driver's chosen gap is combined with their vehicle's on_time. Furthermore, a dual loop detector provides redundant measurements from the paired detectors (Coifman, 1999); however, one must be careful in working with the redundancies. In particular, one could use either the difference in time between when the two detectors turn on (front bumper traversal_time) or when the two detectors turn off (rear bumper traversal_time) to measure speed in Equation 6. In practice the rear bumper traversal_time measurement tends to be noisier than the corresponding front bumper measurement because in many trucks the rear bumper is further

off the ground than the front bumper, leading to less consistent rear bumper transition times for these long vehicles (see, e.g., Coifman, 1999; Wu and Coifman, 2014). For this reason, we exclusively use the front bumper traversal_time to measure speed. Since the upstream detector on_time is measured roughly concurrently with the front bumper traversal_time, we strictly use the upstream detector to measure on_time in this work. Thus, ensuring that the length measurement errors due to vehicle accelerations at low speeds are minimized when using Equation 7 (Wu and Coifman, 2014). Finally, for consistency in Equation 5, h is also measured strictly at the upstream detector.

The clean hypothetical FR curves in Figure 2A were derived from a homogeneous fleet of vehicles with $L_{eff} = 20\ ft$ under stationary conditions, over large sample periods. If the homogeneous fleet has a different L_{eff}, it yields a different curve. To extend the model from Coifman (2014) to homogeneous vehicles with longer L_{eff}, one must recognize that q_o and k_j are functions of L_{eff}. Holding occ_j constant across all L_{eff}, it is a simple exercise to show that given Equation 3, the parameters of qkFR scale as a function of L_{eff} following Equation 8. Meanwhile, from the fundamental equation one can derive the density at capacity, k_o, with the result shown in Equation 9, and this simplifies to Equation 10. Finally, Equation 11 shows the corresponding $occ_o(L_{eff})$ is independent of L_{eff}. Upon using several different values of L_{eff} to recalculate the FR, it gives rise to a family of curves as shown in Figure 2B. The greater L_{eff}, the lower the curve is in this plot, with the top curve corresponding to $L_{eff} = 20\ ft$ and the bottom to $L_{eff} = 73\ ft$.

$$\frac{q_o(L_{eff})}{q_o(20\text{ ft})} = \frac{k_j(L_{eff})}{k_j(20\text{ ft})} = \frac{20\text{ ft}}{L_{eff}} \tag{8}$$

$$k_o\left(L_{eff}\right) = \frac{q_o\left(L_{eff}\right)}{v_f} \tag{9}$$

$$k_o\left(L_{eff}\right) = \frac{q_o(20\ ft)}{v_f} * \frac{20\text{ ft}}{L_{eff}} = k_o(20\ ft) * \frac{20\text{ ft}}{L_{eff}} \tag{10}$$

$$occ_o\left(L_{eff}\right) = k_o\left(L_{eff}\right) * L_{eff} = k_o(20\ ft) * 20\text{ ft} = \text{occ}_\text{o}(20\ ft) \tag{11}$$

From Equation 11 it should be clear that the speed-occ FR (voccFR) in this hypothetical model is independent of L_{eff}. Thus, as shown with the dashed line in the qoccFR on the right of Figure 2B, all seven curves exhibit the 15 mph point just below 40% occupancy even though L_{eff} ranges from 20 to 73 ft with the corresponding q ranging from 1,500 vph to 500 vph. With real traffic the corresponding speed across different vehicle lengths might not fall in a perfect column like this figure, a point we will revisit in Section 4. For now it is sufficient to note that the hypothetical models are used strictly for reference, the empirical calculations do not depend on an underlying model.

A conventional fixed time period sample is really just an inhomogeneous average of several vehicles of different lengths and speeds. This inhomogeneous sample effectively corresponds to drawing a weighted average from the corresponding qoccFR(L_{eff}) curves in Figure 2B, leading to considerable noise in the traffic state measurement. As shown in Figure 3, in the queued regime a change in L_{eff} leads to a vertical displacement in the q-occ plane (or in the case of qkFR, radial from the origin), while a change in v leads to a displacement with a negative slope in the q-occ plane, following the given qoccFR curve. With these two competing translations, it is impossible to separate the impacts of length from the impacts of speed on conventional fixed time period traffic state measurements. Unfortunately most empirical FR studies do not contemplate the impacts of inhomogeneous vehicles, or if they do, it is typically

only to the depth of passenger car equivalents (PCE). However, as shown in Coifman (2014), PCE is far too simplistic to address the impacts of different values of L_{svp}. A few studies have tried to address this issue, with one of the best examples being Persaud and Hurdle (1988). They explicitly used a lane with a truck restriction to avoid, "the complication of determining and applying passenger car equivalency conversions." Even though Persaud and Hurdle excluded trucks, it is likely that their data still included other long vehicles like buses and automobiles pulling trailers.

To minimize the impacts arising from a large range of vehicle lengths in our new methodology to derive an empirical FR, the vehicles are sorted into L_{svp} bins that only span 5 or 10 ft. A total of 10 bins were used in this study, consisting of the seven bins in the legend of Figure 2B, a 16-18 ft bin, *below 16 ft* bin, and *above 78 ft* bin.[2] The vehicles in each length bin are then treated separately from the other length bins. To minimize the impacts of different speeds, the vehicles in a given length bin are further sorted into v_{svp} bins that only span 1 mph. To minimize the impacts of detector errors, any vehicle meeting any one of the three following criteria is excluded because its measured h may not be representative of an actual vehicle passage:

- following an unmatched pulse,[3] as characterized by two successive pulses at either the upstream or downstream detector in the dual loop without an intervening pulse at the other detector (Coifman and Cassidy, 2002) since the real lead vehicle may have passed undetected,
- involved in a suspected pulse breakup, as characterized by an infeasibly short off time between two successive pulses at a given detector (Lee and Coifman, 2011) since the on-time and h are likely inaccurate, or
- following a suspected pulse breakup, since the lead vehicle's rear bumper passage time may have been measured prematurely.

To ensure the largest possible number of similar vehicles per sample, the median q_{svp} and median occ_{svp} are found for each combined length and speed bin. Thus, this clustering approach groups vehicles based on similar speed and length, without regard to arrival order. This use of the median is also important. Most conventional traffic state measurements use the mean rather than the median to find the center of the given distribution. Yet the mean is far more sensitive than the median to outliers that are common in empirical traffic data (see, e.g., Coifman, et al., 2003). The outliers arise both due to occasional detector errors that are not caught and due to uncommon driver behavior (e.g., the distribution of feasible headways is skewed- it is possible for a driver to take a headway many times larger than average, but the driver cannot go smaller than a fraction of the average headway).

3. Application

Using the exact same individual vehicle actuations used to derive Figure 1, the plot in the first column of Figure 4 shows q_{svp} versus occ_{svp} for each of the 20,175 individual vehicles that

[2] Since the effective vehicle length measurement depends on the loop geometry, the length bins may have to be redefined to account for this fact when applying this work to a new location.

[3] Where a "pulse" denotes one detector's response to one vehicle, i.e., from the time the loop turns on in response to the front bumper to the time it turns off in response to the rear bumper.

passed in the given lane on the given day (after excluding unmatched pulses, detector errors, etc.). As expected, this plot shows considerably more scatter than Figure 1A. For reference, Figure 4 repeats the dashed line at q_P = 1,500 vph, as was used in Figure 1.

We use L_{svp} to sort each svp measurement into one of 10 different length bins, with the resulting plots for three of the length bins shown in the second column of Figure 4. Note how the slope of the free flow regime (left-hand edge of the point cloud) decreases as L_{eff} increases, consistent with the hypothetical example in Figure 2B. Throughout this figure the total number of vehicles, N, in each plot is shown above the given plot. The middle row of the first two columns show that on this day over two thirds of the vehicles fall in the 18-22 ft bin, corresponding to passenger vehicles. Taking all of the vehicles in a single L_{svp} bin, we use the given vehicle's v_{svp} to sort it into one of 70 speed bins, with the resulting plots for three of these speed bins from the 18-22 ft vehicles shown in the third column of Figure 4. We then take the median(q_{svp}) and median(occ_{svp}) for each one of these combined length and speed bins, as shown with a dark point in each of the third column's plots. Plotting the curve passing through the median values across all speed bins for a given length bin, the final column of Figure 4 shows the resulting measured qoccFR on this day. Ultimately we will follow this same process for the other L_{svp} bins too. However, the other L_{svp} bins typically have far fewer vehicles in them, and so for the moment our discussion will focus strictly on the passenger vehicles, as shown with shaded region surrounding the five plots on the right of the figure.

Figure 5A superimposes the measured qoccFR from the final column of Figure 4 on top of the corresponding T=30 sec samples from Figure 1A. Figure 5B repeats the process from an additional 17 days at this dual loop detector, each taken individually (for a total of 18 days, all from the same month)[4]. This plot shows the reproducibility of the measured qoccFR across days. Note that the lowest speeds in the individual qoccFR are erratic due to two factors: (1) very few vehicles past at these speeds on a given day. (2) As discussed in Coifman (2014) measurement errors increase as speeds decrease, to the point that for measured v_{svp} below 5 mph a vehicle can come to a complete stop for an unknown amount of time, potentially rendering the corresponding occ_{svp} meaningless. Above 5 mph, the measured qoccFR traces out the trapezoidal shape predicted by Hsu and Banks (1993), with a roughly linear congested regime between 5 mph and the threshold q_P due to downstream inflow consuming a portion of the bottleneck capacity, and then a roughly horizontal curve between queued and unqueued at q_P (actually in this case, the horizontal curve falls slightly above q_p due to the nature of the sampling process). Of course the measurements for q above q_P should not be transferrable to other locations that do not have similar downstream inflow, so like the lowest speed data, we recommend treating these regions with extra scrutiny (as we will do shortly, in subsequent figures).

Recall that over two thirds of the vehicles fall in the 18-22 ft length bin, and thus, the other length bins typically have far fewer vehicles in the congested regime on a given day (see, e.g., N for the other two plots shown in the second column of Figure 4). To increase the sample size and smooth out the noise in the daily curves, we use all 18 days to first find a single median q_{svp} and occ_{svp} for a given combined length and speed bin (analogous to the third column of Figure 4 except now using svp data from 18 days combined to find the median values instead of

[4] These data come from BHL station 6, westbound, on I-80, just north of Oakland, California, collected December 6th to 23rd, 1997. Each day of data includes a full 24 hrs. Many other dates and locations were considered in this work, with all of the other data sets being more recent. We found consistent results across the various datasets; however, we have chosen to present the December 1997 data because it has the greatest amount of queued traffic, with most of the 18 days experiencing over 12 hrs of recurring congestion due to high demand and a series of downstream bottlenecks. Only one of the days experienced less than 6 hrs of recurring congestion.

just one day of svp data) and the dark curve in Figure 5C shows the median values across all speed bins for the 18-22 ft vehicles, i.e., the measured qoccFR for this length bin over the 18 days in this lane. For reference, the 18 curves from the individual days from Figure 5B are repeated in a lighter shade on Figure 5C.

Thus far the analysis has focused on a single lane (lane 4, the shoulder lane) at this directional detector station. Figure 6 repeats the process from Figure 5C for the 18-22 ft length bin, individually by lane for all four lanes at the station over the same 18 days. The curves for the different lanes only diverge above the q_P threshold (shown with a dashed line). Below q_P the four lanes exhibit very similar qoccFR curves.

Combining all of the individual vehicle actuations from all 4 lanes and all 18 days, we calculate a single measured qoccFR for each length bin, across all of the corresponding speed bins. The right-hand side of Figure 7A shows the resulting curves by length bin subject to the following three exclusions:

(1) To remove the impacts of the downstream inflow, all speeds in all length bins that result in q above the threshold q_P for the 18-22 ft length bin are suppressed (as per the corresponding qvFR in the left-hand side of Figure 7A).
(2) To remove the impacts of the measurement errors at low speeds, all speeds below 5 mph in all length bins are suppressed.
(3) To remove the impacts of small sample sizes, all combined length and speed bins with fewer than 100 vehicles are suppressed.

As a result of the third exclusion, only seven length bins remain with sufficient data. The seven curves are distinctly visible in the q-v plane on the left-hand side of Figure 7A. The length range increases from the top curve to the bottom curve in this plot. On the right-hand side the two shortest length bins remain distinct, but the curves from the five longest bins overlap, in part due to the vertical compression as L_{eff} increases, evident in Figure 2B; in part due to smaller sample sizes in these length bins; in part due to the fact that the speed measurement errors from exclusion (2) are greater for longer vehicles simply because they are over the detector for a longer amount of time; and in part due to the fact that the actual speed-occupancy relationship appears to exhibit a slight dependency on L_{eff} for these longer vehicles, leading to a small lateral shift in the right-hand side of Figure 7A. Except from the small lateral overlap, all of the curves exhibit trends consistent with the hypothetical example in Figure 2B. Although the speed range on Figure 7A is relatively small, 5 mph to 17 mph, the occ range spans roughly a quarter of the observable values below jam occupancy (as per the distortions of the q-occ plane discussed in Coifman, 2014).

The dotted curves in Figure 7B relax exclusion (1), lifting the upper bound speed exclusion to 50 mph and eliminates the lower bound speed, exclusion (2), altogether (for reference, the curves from Figure 7A are repeated in bold). In the right-hand side of Figure 7B the measured qoccFR curves for most of the length bins flatten out at higher q (corresponding to higher v), i.e., in the region above the threshold q_P from the downstream inflow, shown with a dashed line in these plots. For the shortest length bin (again, accounting for over two thirds of the vehicles) the curve now extends measurements down to 1 mph. The curve remains roughly straight throughout this low speed region, possibly indicating that with a sufficiently large sample size the median is not very sensitive to the outliers arising from the dual loop detector measurement limitations for these very low speeds. If so, the resulting occ range for speeds

between 1 and 4 mph covers an additional quarter of the feasible values of occ, with the combined speed range from 1 mph to 17 mph covering more than half of the feasible occ values.

3.1. Single loop detectors

This methodology is primarily intended for application to data from dual loop detectors[5] rather than single loop detectors because the impacts of an individual vehicle's speed and length cannot be separated in the single loop detector measurements. However, most urban freeways in the US are characterized by a high percentage of passenger vehicles that fall over a small range of lengths. For a location like that, one can use the speed estimation method from Coifman et al (2003) to take a moving median of on_time to estimate individual vehicle speeds via Equation 12, where L_{pax} is set to 20 ft. So even though one cannot isolate the passenger vehicles, because they are by far the dominant flow, the median will excluded the impacts from the long vehicles in the speed estimate and thus, the estimated speeds can also be used to estimate vehicle length even in queued traffic. If one did not bin vehicles by length and instead found the qoccFR across all vehicles, then the passenger vehicles will still dominate the median(q_{svp}) and median(occ_{svp}) in each speed bin.

$$v_{svp} = \frac{L_{pax}}{median(on\_time)} \tag{12}$$

Of course there will also be occasional extreme outlier measurements in the svp calculations. To accommodate this fact with the single loop detectors, L_{svp} is calculated from Equation 7 (except now using Equation 12 to estimate speed instead of measuring it from Equation 6) and only one length bin is retained, with the goal of finding just the passenger vehicles. The speed estimates From Equation 12 are good, but not as good as the dual loop measurements from Equation 6, so when using single loops one should allow more tolerance for speed variations. Thus, the range of the passenger vehicle length bin is set larger than was used for dual loop detectors. Again, the longer vehicles are by far in minority so including some of them in the bin should have little impact on the median calculations, and the single loop data does not have sufficient resolution to consider any of the less common vehicle lengths.

Figure 8 repeats the analysis from Figure 7B using strictly the single loop detector measurements from the upstream loop in the given dual loop detector. It uses a moving median of 11 vehicles centered on the given vehicle to find v_{svp} and a single length bin of 16 - 28 ft to capture only the passenger vehicles. For reference, the figure also shows the results from the dual loop detector for the 18 - 22 ft bin. The single loop curves are very similar to the dual loop curves for speeds above 5 mph (the lower end of the bold curves). Below 5 mph they diverge due to the limitations of Equation 12 (estimated speeds in this range can erroneously be measured too low, but they are not countered by even lower true speeds being estimated too high). The analysis was repeated on a lane by lane basis and there too, the single loop results were similar to the dual loop results for speeds above 5 mph.

[5] Or detectors/methods that emulate the functionality of a dual loop detector, e.g., manually measuring vehicle passages from video.

4. Discussion and Conclusions

This paper revisited the process of deriving an empirical fundamental relationship from detector data. Our new methodology seeks to address several sources of noise present in conventional measures of the traffic state arising from the aggregation process, as were discussed in Coifman (2014). In this new methodology vehicles are no longer taken successively in the order in which they arrived and there is no requirement to seek out stationary traffic conditions; rather, the traffic state for each vehicle is measured individually using Equations 4-7 and these measurements are grouped by similar lengths and speeds before aggregation. They are then binned by length and speed, with each length bin spanning 5 or 10 ft, and speed bin spanning 1 mph increments. Care is also taken to exclude vehicle measurements that might be corrupted by detector errors.

Conventional aggregation techniques find the average traffic state over a small number of inhomogeneous vehicles and typically include a non-integer number of headways. Whereas our new methodology ensures a large set of homogeneous vehicles and speeds, measured with an integer number of headways. For each length bin we then calculate the median flow and median occupancy in each speed bin and connect these points to generate the qoccFR curve for the given length bin, or use the corresponding v to generate the qvFR curve. This use of the median is also important, unlike conventional aggregation techniques that find the average; the median is far less sensitive to outliers arising from occasional detector errors or uncommon driver behavior.

Figure 5 shows consistent results across 18 independent days at one detector, Figure 6 shows consistent results across 4 independent lanes at one detector station, and Figure 7 shows consistent results across 7 independent length bins. Of note is the fact that the empirical results in Figure 7 collected under non-stationary traffic are consistent with the hypothetical results generated under stationary traffic conditions in Figure 2B. There is no complicated filtering beyond taking the median values in each bin. Rather, the strong performance of this new method is due to the fact that this approach takes great care to preserve an integer number of headways in each measurement, and then bins the individual measurements to ensure a large number of observations, with homogeneous vehicle length and speed before aggregation.

The distortions of the q-occ plane discussed in the context of Figure 2A are readily apparent in Figure 7, as follows. The speed range in Figure 7A spans roughly 18% of the feasible speeds (5 mph $\leq$ v $\leq$ 17 mph), but these data span roughly 25% of the feasible q and occ. As shown in Figure 7B, if one extends the range to 1 mph $\leq$ v $\leq$ 17 mph (roughly 26% of the feasible speeds) the data now span more than 50% of the feasible q and occ measurements.

Figure 7 also shows some evidence that the actual voccFR may depend on L_{eff}, leading to a small lateral shift for the longer vehicles in the right-hand side of Figure 7A. Recall that the derivation of Figure 2B assumed that occ_j remained constant across L_{eff}. Thus, assuming that longer vehicles will come to a stop with a longer spacing than the shorter vehicles. If instead, one assumed that all vehicles came to a stop with a constant physical gap between vehicles, the hypothetical model for the homogeneous vehicles from Section 2 should be revised as follows. The parameters of qkFR now scale as a function of L_{eff} following Equation 13. Thus, via Equation 2, occ_j and occ_o now become functions of L_{eff}, given by Equations 14-15. Using the same parameters from Figure 2, the resulting qvFR and qoccFR for the hypothetical example are shown in Figure 9. Notice in the qoccFR the curves corresponding to different lengths now cross over one another at high occ because occ_j increases with L_{eff}. Thus, providing a potential mechanism for the small lateral shift at longer L_{eff} in Figure 7. In the context of Figure 3A, a change in L_{eff} would now lead to a displacement with a negative slope in the q-occ plane, further

obscuring the separate impacts of length and speed in conventional fixed time period traffic state measurements.

$$\frac{q_o(L_{eff})}{q_o(20\text{ ft})} = \frac{k_j(L_{eff})}{k_j(20\text{ ft})} = \frac{20\text{ ft}+gap}{L_{eff}+gap} \tag{13}$$

$$occ_j(L_{eff}) = occ_j(20\ ft) * \frac{20\text{ ft}+gap}{L_{eff}+gap} * \frac{L_{eff}}{20\ ft} \tag{14}$$

$$occ_o(L_{eff}) = occ_o(20\ ft) * \frac{20\text{ ft}+gap}{L_{eff}+gap} * \frac{L_{eff}}{20\ ft} \tag{15}$$

The hypothetical models are used strictly for reference in this paper, the exact form is not critical since the empirical measurements that are the focus of this paper do not depend on an underlying model. That said, it is unlikely that either of the simple hypothetical models fully capture the dependency on L_{eff}, rather, longer vehicles probably do take longer gaps when stopping, but not typically in direct proportion to L_{eff}. With a greater understanding of these dynamics (the subject of on-going research) it may be possible to fine tune traffic flow or car following models to account for such subtle influences and better predict traffic behavior.

Historically there have been at least three sources of noise in measuring empirical FR: errors due to aggregating vehicles together, errors due to the detector settings, and variability due to site specific traffic behavior. All too often the aggregation errors swamped out the other two sources, particularly at low speeds. Having now accounted for most of the aggregation errors, the two remaining sources should become much more apparent; however, the magnitude of these two remaining sources of noise should be no larger with the new method than it has been in past methods. Nonetheless, future work should investigate the impacts of the loop detector calibration, e.g., L_{eff} depends on the sensitivity setting and responsiveness of the given loop detector (Lee and Coifman, 2012). These factors will likely result in slightly different empirical curves from one loop detector station to another simply due to the detector settings rather than actual traffic behavior. Of course there are also site-specific traffic behavior that is non-transferrable, e.g., in this case the downstream inflow truncating the upper portion of the qoccFR to q_P. Or more generally, there could be other site specific issues, time of day factors, or transient events that cause the FR to change (e.g., the 18 qoccFR curves from different days in Figure 5B are consistent but not identical). So here too, future work should examine these factors in detail. Of course this latter point is the ultimate goal traffic flow theory: to better understand the factors that determine driver behavior and traffic flow. By stripping away most of the aggregation errors this paper has brought us one step closer to realizing that goal.

It is also important to note that this is a study of qoccFR, not of qkFR. From the discussion in Section 2 of Figure 3 and PCE one should be very careful about generalizing from occ to k without knowing the individual vehicle lengths in the given sample. Further underscoring this difference, the slope in the queued regime of qoccFR for the two hypothetical models depend on L_{eff} (as per the right-hand side of in Figures 2B and 9). Yet for both hypothetical models the slope of the queued regime of the qkFR should be constant, independent of L_{eff} due to the constraints from Equations 8 and 13. So aside from reiterating the caution from Persaud and Hurdle (1988) about PCEs, this paper provides no guidance on how signals and waves should propagate in LWR or other traffic flow models.

The first application of this work is likely to be generating much cleaner empirical qoccFRs. From which one can then derive more precise models and simulations. Although it is not yet clear how best to deal with inhomogeneous vehicle lengths, the technique presented

herein should prove to be an important tool to help find the answer. In the mean time, the curves for 18-22 ft vehicles in Figures 6 and 7B should be immediately useful for studies of passenger vehicles.

References

Cassidy, M. (1998) "Bivariate Relations in Nearly Stationary Highway Traffic," *Transportation Research Part B*, Vol. 32, No. 1, p. 49-59.

Chandler, R.E., Herman, R., Montroll, E.,W., (1958) "Traffic dynamics: studies in car following," *Operation Research*, Vol. 6, No. 2, pp. 165-184.

Coifman, B. (1999) "Using Dual Loop Speed Traps to Identify Detector Errors," *Transportation Research Record 1683*, Transportation Research Board, pp 47-58.

Coifman, B. (2001) "Improved Velocity Estimation Using Single Loop Detectors," *Transportation Research: Part A*, Vol 35, No 10, pp 863-880.

Coifman, B. (2014) "Jam Occupancy and Other Lingering Problems with Empirical Fundamental Relationships," [in press] *Transportation Research Record*.

Coifman, B., Cassidy, M. (2002) "Vehicle Reidentification and Travel Time Measurement on Congested Freeways", *Transportation Research: Part A*, vol 36, no 10, 2002, pp. 899-917.

Coifman, B., Dhoorjaty, S., Lee, Z. (2003) "Estimating Median Velocity Instead of Mean Velocity at Single Loop Detectors," *Transportation Research: Part C*, Vol 11, No 3-4, pp 211-222.

Coifman, B., Lyddy, D., Sabardonis, A. (2000) "The Berkeley Highway Laboratory- Building on the I-880 Field Experiment," *Proc. IEEE ITS Council Annual Meeting,* IEEE, pp. 5-10.

Gazis, D., Foote, R. (1969). "Surveillance and Control of Tunnel Traffic by an On-Line Digital Computer," *Transportation Science*, Vol 3, No 3, pp 256-275.

Gazis, D. C., Herman, R., Rothery, R. W., (1961) "Nonlinear follow the leader models of traffic flow," *Operations Research*, Vol. 9, No. 4, pp. 545-567.

Hsu, P., Banks, J., (1993) "Effects of Location on Congested-Regime Flow-Concentration Relationships for Freeways," *Transportation Research Record 1398*, pp 17-23.

Hurdle, V.F., Datta, P. K., (1983). "Speeds and flows on an urban freeway: some measurements and a hypothesis." *Transportation Research Record No. 905*, 127-137.

Lee, H., Coifman, B., (2011) "Identifying and Correcting Pulse-Breakup Errors from Freeway Loop Detectors," *Transportation Research Record 2256*, pp 68-78.

Lee, H., Coifman, B., (2012) "Quantifying Loop Detector Sensitivity and Correcting Detection Problems on Freeways," *Journal of Transportation Engineering, ASCE,* Vol. 138, No. 7, pp 871-881.

Lighthill, M., Whitham, G., (1955) "On Kinematic Waves II. a Theory Of Traffic Flow on Long Crowded Roads, "*Proc. Royal Society of London, Part A*, Vol. 229, No. 1178, pp 317-345.

Persaud, B., Hurdle V. (1988) "Some New Data That Challenge Some Old Ideas About Speed-Flow Relationships," *Transportation Research Record 1194*, p. 191-198.

Richards, P., (1956) "Shock Waves on the Highway," *Operations Research*, Vol. 4, No. 1, pp 42-51.

Wu, L., Coifman, B., (2014) "Vehicle Length Measurement and Classification in Congested Freeway Traffic," [in press] *Transportation Research Record*.

List of Figures

Figure 9, Repeating Figure 2B only now assuming the intra-vehicle gap at jam remains constant across fleets. The dashed line shows that a given v corresponds to different occ across different L_{eff}.

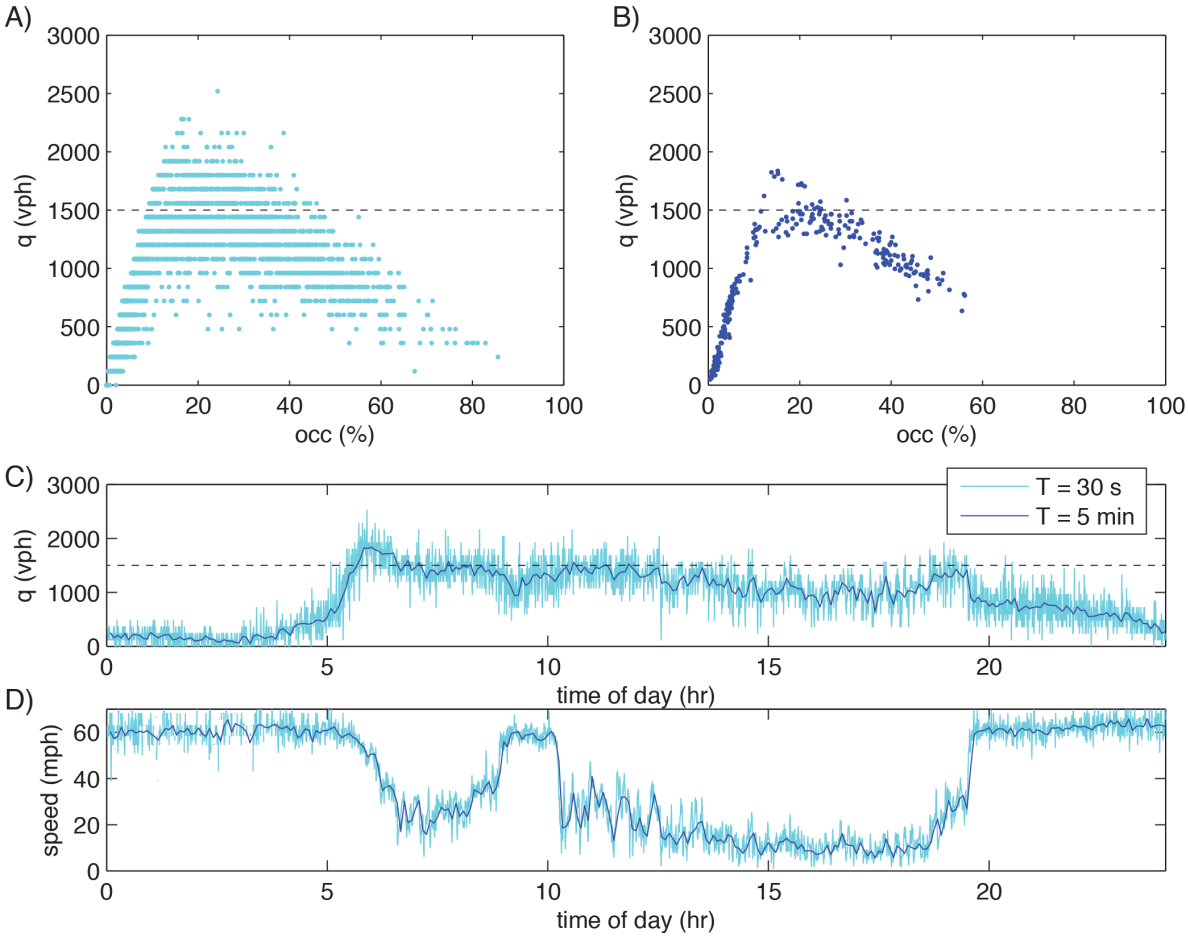

Figure 1, Conventional q versus occ (A) T = 30 sec, (B) T = 5 min. The corresponding time series (C) flow, and (D) speed. For reference a dashed line is shown at q_P = 1,500 vph.

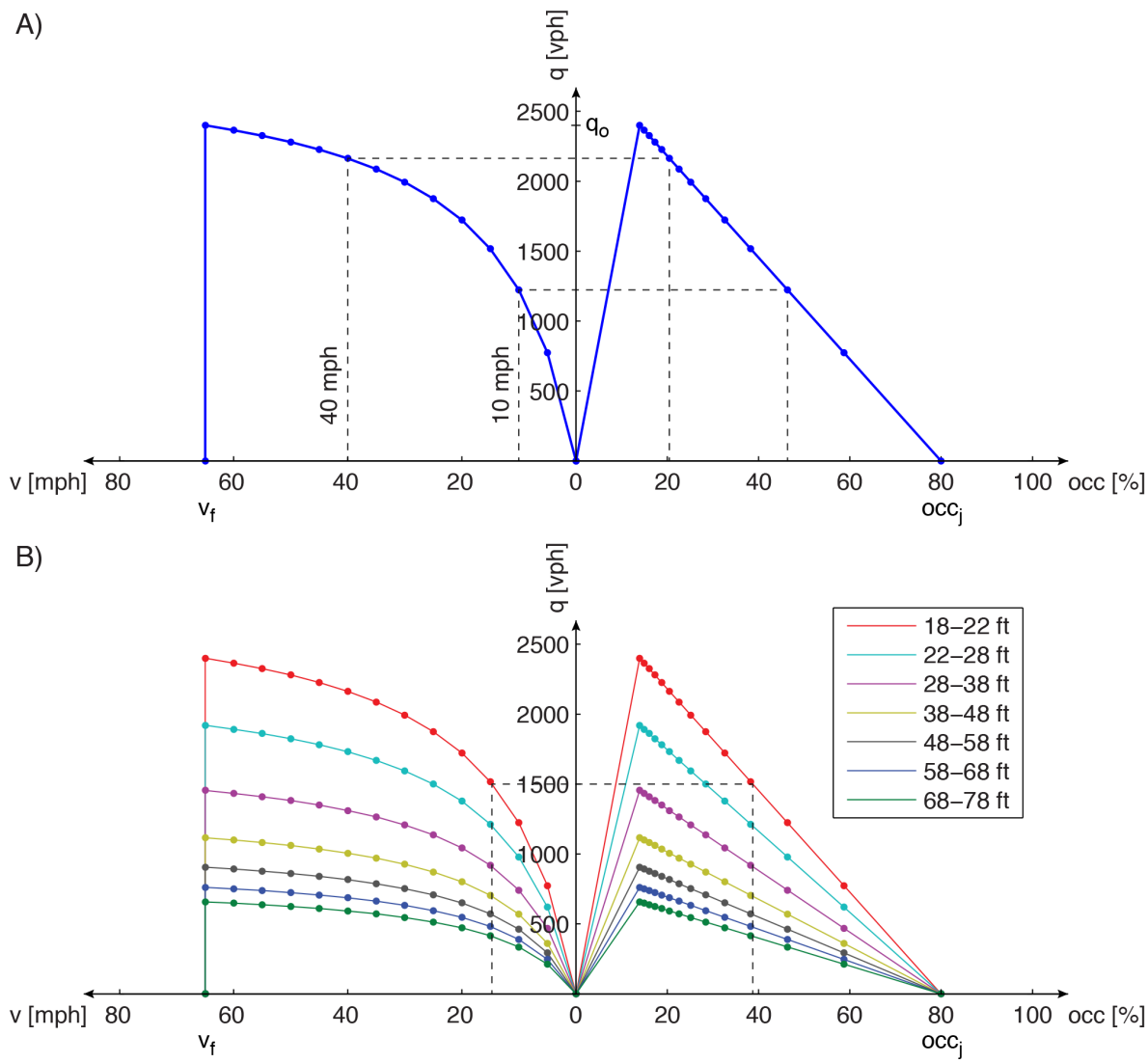

Figure 2, (A) Fundamental relationship between flow versus speed (on the left) and flow versus occupancy (on the right) for a homogeneous fleet of passenger vehicles with L_{eff} = 20 ft under stationary conditions and very long sampling periods. (B) Extending the relationship to homogeneous fleets with longer lengths, from passenger vehicles (L_{eff} = 20 ft) to dual unit trucks (L_{eff} = 73 ft) assuming occ_j remains constant across the fleets. The dashed line shows that a given v corresponds to the same occ across different L_{eff}.

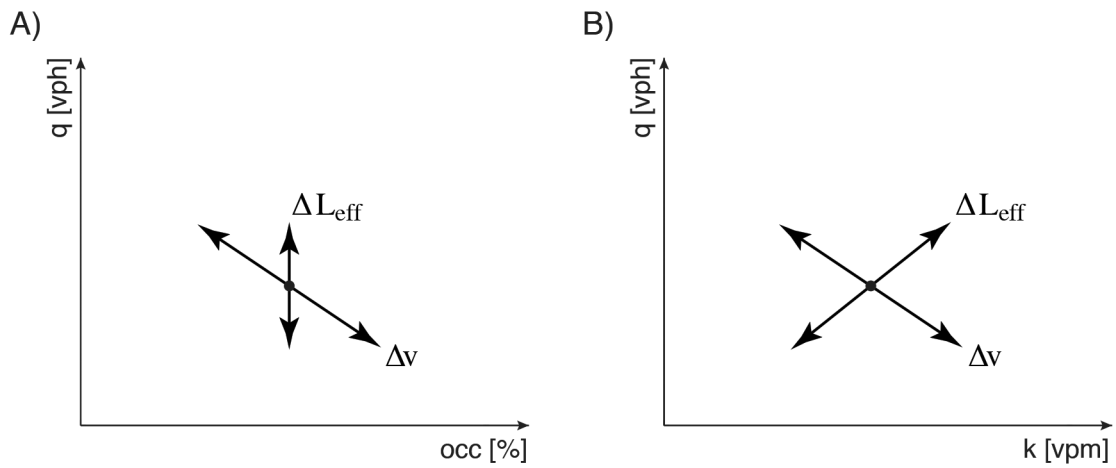

Figure 3, The impacts of changes in L_{eff} and changes in v on the measured traffic state in the queued regime of (A) the flow-occupancy plane, and (B) the flow-density plane.

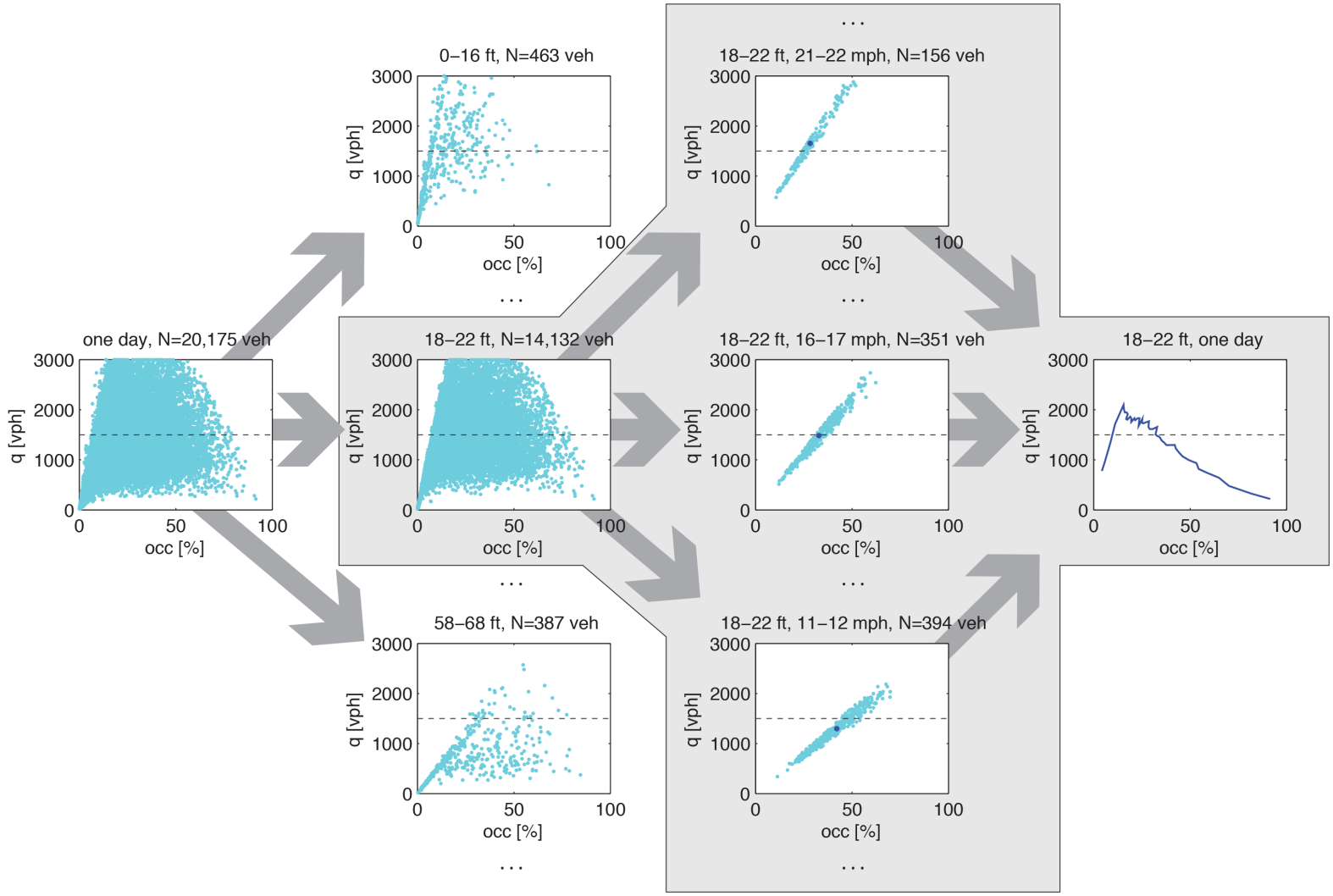

Figure 4, The left plot shows q_{svp} versus occ_{svp} for all vehicles previously used to generate Figure 1. The second column sorts these vehicles by length bin (three length bins shown). Within each length bin the vehicles are further sorted by speed bin (three speed bins shown, all from the 18-22 ft length bin) and the median q and occ is shown with a dark point in each plot. The final column shows the resulting qoccFR the 18-22 ft length bin after connecting the median points from the third column of plots. The specific bin(s) and number of vehicles, N, are shown above each plot. For reference a dashed line is shown at q_P = 1,500 vph.

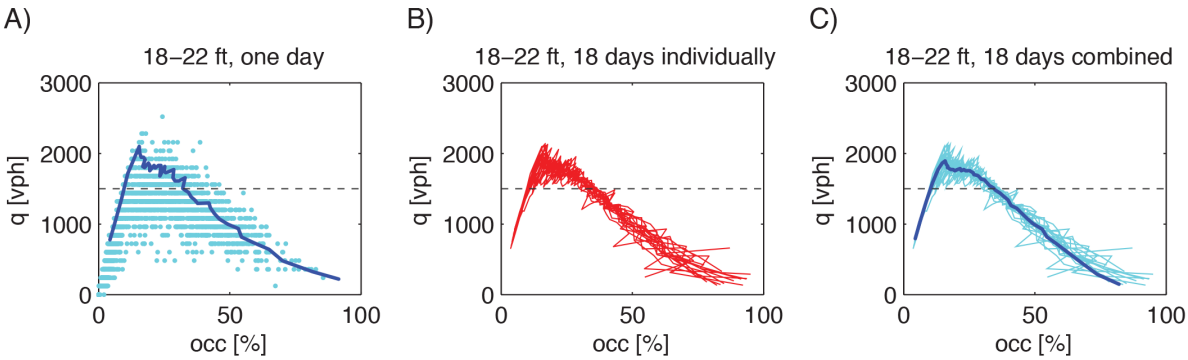

Figure 5, (A) The qoccFR for the 18-22 ft length vehicles from Figure 4 and the corresponding T = 30 sec q versus occ from Figure 1A for the given lane and day. (B) Repeating the daily qoccFR calculation across 18 days for the 18-22 ft length vehicles in the given lane. (C) Recalculating qoccFR by combining all 18 days before finding the median values for the 18-22 ft length vehicles, with the individual daily curves shown in a lighter shade for reference. Consistent with earlier figures, a dashed line is shown at q_P = 1,500 vph for reference.

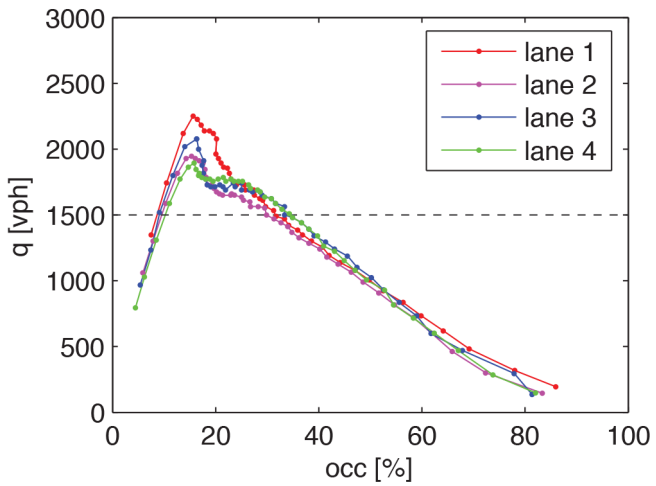

Figure 6, Repeating Figure 5C applied independently by lane, across the four lanes at the directional detector station (lane 1 is the median lane, and lane 4 the shoulder).

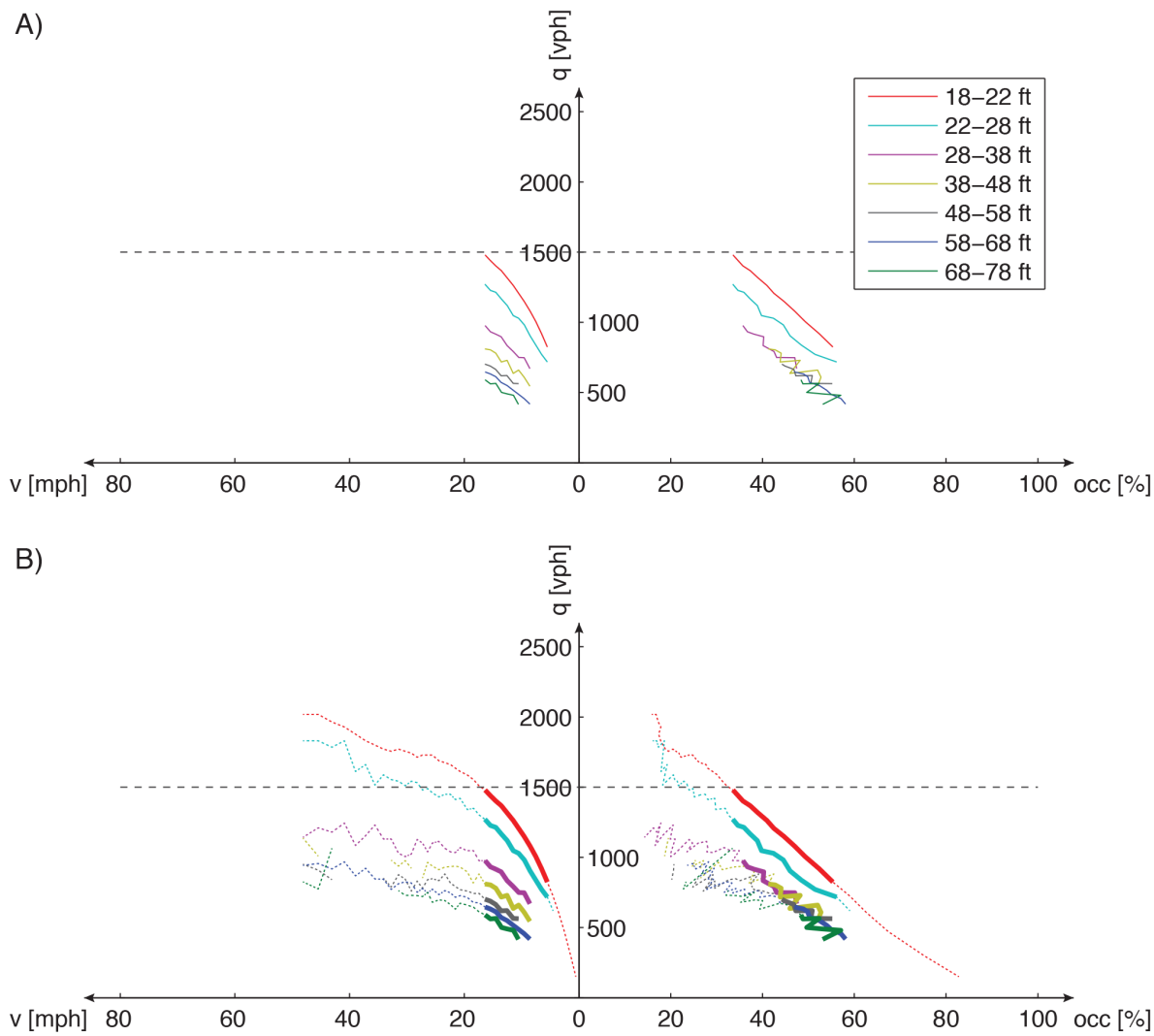

Figure 7, The resulting qvFR and corresponding qoccFR using the process from Figure 4, applied to the svp data for each length bin individually using the data from all 18 days and all four lanes combined together for (A) 5 mph to 17 mph, and (B) 1 mph to 50 mph. Compare to the hypothetical example in Figure 2B. Once more, a dashed line is shown at q_P = 1,500 vph for reference.

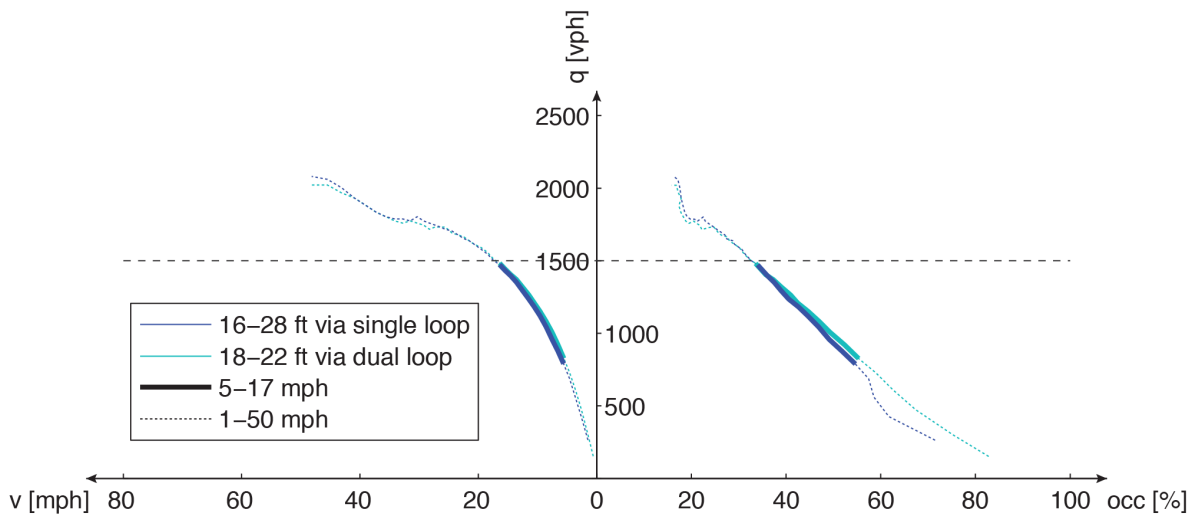

Figure 8, Repeating the analysis from Figure 7B for passenger vehicles using strictly the single loop detector measurements. For reference, the figure also uses a lighter shade to show the corresponding results from the dual loop detector.

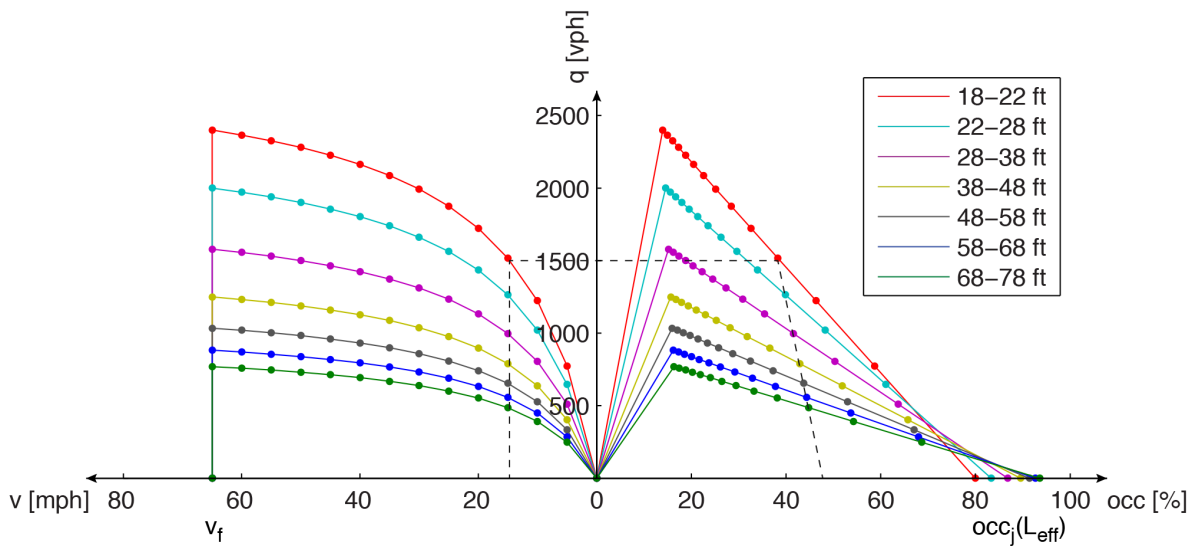

Figure 9, Repeating Figure 2B only now assuming the intra-vehicle gap at jam remains constant across fleets. The dashed line shows that a given v corresponds to different occ across different L_{eff}.